*Exploration Geophysics (1995) **26**, 186-194*

Resistivity imaging by Time Domain Electromagnetic Migration (TDEMM)

Michael S. Zhdanov
University of Utah
Department of Geology
and Geophysics
Salt Lake City, UT 84112

Peter N. Traynin
University of Utah
Department of Geology
and Geophysics
Salt Lake City, UT 84112

Oleg Portniaguine
University of Utah
Department of Geology
and Geophysics
Salt Lake City, UT 84112

ABSTRACT

One of the most challenging problems of electrical geophysical methods is the interpretation of time domain electromagnetic (TDEM) sounding data in the areas with the horizontally inhomogeneous geoelectrical structures. This problem is of utmost importance in mining exploration and environmental study, in particular, in the case of sounding conducted in the transmitter offset or slingram mode. The conventional 1D EM inversion technique cannot solve this problem, because the observed data are strongly distorted by horizontal conductivity inhomogeneities. The multidimensional EM inversion techniques existing today can handle only simple models, require repetitive forward modeling solutions, and therefore are very time consuming.

We developed a new approach to the interpretation of TDEM data over inhomogeneous structures based on downward extrapolation of the observed electromagnetic field in reverse time (*the time domain electromagnetic migration*). Numerical solution of this problem is provided by an electromagnetic analog of the Rayleigh integral. TDEM migration transforms EM data, observed on the surface of the Earth, into immediate geoelectrical images of geological cross sections. This transformation is very fast (requiring only a few seconds of CPU time on PC) and stable to the random noise in the data.

The numerical results of rapid inversion based on the time domain electromagnetic migration illustrate the property of migration described above. This method has also been applied to waste site characterisation. We have analysed the data obtained as a result of high density TDEM profiling survey with the Geonics EM47 along the set of profiles, intersecting Cold Test Pit waste site within the Radioactive Waste Management Complex (RWMC) at the Idaho National Engineering Laboratory (INEL). Time domain electromagnetic migration and resistivity imaging made it possible to outline the conductive sections of the pit filled with the waste.

INTRODUCTION

This paper focuses on improving the analysis and imaging of time domain electromagnetic (TDEM) data. In the past these data were processed using a simplified technique based on the 1D apparent resistivity calculation. This technique works well enough for horizontally homogeneous structures. There are several publications dedicated to the development of simple and fast inversion techniques for the processing of transient EM data over inhomogeneous structures (Eaton and Hohmann, 1989), (Macnae and Lamontagne, 1987), (Barnett, 1984). The majority of these papers have been based on equating the transient response, measured at the surface of the Earth, to the EM field of current filament images of the source. This approach originated in the pioneering work of Nabighian (1979) who described the behaviour of transient currents diffusing into the Earth as a system of "smoke rings" blown by the transmitting loop into the Earth.

In this paper we develop and test a different approach to processing transient data, based on downward extrapolation in reverse time. We call this method *time domain electromagnetic migration* (Zhdanov et al. 1994), (Zhdanov and Booker, 1993). It results from transforming the observed data to a geologically meaningful image of the geoelectrical cross section.

The basic principles of EM migration have been formulated in (Zhdanov, 1988), (Zhdanov et al, 1988), (Zhdanov and Keller, 1994), and Zhdanov et al. 1994). EM migration has important features in common with seismic migration (Zhdanov et al, 1988), (Claerbout, 1985), but differs in that for geoelectric problems, EM migration is done on the basis of a diffusion equation rather than a wave equation.

Let us consider the case in which we have observed an EM field produced by a controlled source over an array of receivers. The array of receivers will be situated on the surface of the Earth for this discussion. Having recorded time-varying EM field components over the array of receivers, we then conceptually replace the receivers with an array of sources, each driven with a moment which replicates the actually recorded time-varying field components. The conceptual sources are driven in reverse time to produce a field that we call the *migrated EM field.* Like in the seismic case, this field can "illuminate" the internal structure of the Earth and give us a "geoelectric image" of the Earth's interior.

Time domain EM migration (TDEMM) is based on the downward extrapolation of the observed EM field in reverse time. Numerical solution of this problem is provided by an EM analog of the Rayleigh integral, that, in exact analogy with a seismic problem, produces upgoing fields (i.e. fields propagating in the direction of the observation surface). These

upgoing fields are EM analogues of the upgoing Claerbout seismic waves and, consequently, can feature some of the properties of the latter. For example, for imaging the geoelectrical cross-section we can use the "EM radiating-inhomogeneities" concept, analogous to the exploding- reflectors concept, widely used in seismic migration. According to this concept the position of secondary sources of the EM field (geoelectric inhomogeneities - boundaries, anomalous conductive or isolating zones) can be determined according to the position of the extreme point of the migrated field.

We also developed a technique for transforming the EM migration fields and their different components into resistivity images of the vertical cross-section.

In this paper we present the theoretical foundations of EM migration and resistivity imaging and illustrate them by the results of numerical modeling and the interpretation of the time domain EM (TDEM) data set acquired at the Cold Test Pit site within the Radioactive Waste Management Complex (RWMC) at the Idaho National Engineering Laboratory (INEL).

TIME DOMAIN ELECTROMAGNETIC MIGRATION

Consider a model in which the horizontal plane, z=0 separates the conductive Earth ($z>0$) from the insulating atmosphere ($z<0$). The conductivity in the Earth, $\sigma(\vec{r})$, is represented as the superposition of a constant normal conductivity, σ_n=*const*, and an anomalous conductivity function, $\Delta\sigma(\vec{r})$:

$$\sigma(\vec{r}) = \sigma_n + \Delta\sigma(\vec{r}) \tag{1}$$

Everywhere in the Earth outside the anomalous region, the magnetic $\vec{H}$ and electric $\vec{E}$ fields satisfy the diffusion equation:

$$\Delta\vec{H} - \mu_0\sigma_n\frac{\partial\vec{H}}{\partial t} = 0, \quad \Delta\vec{E} - \mu_0\sigma_n\frac{\partial\vec{E}}{\partial t} = 0 \tag{2}$$

where μ_0 is the magnetic permeability of free space.

For this model, we can discuss the problem of migration of any scalar component, $P(\vec{r},t)$, of an observed EM field.

We define the *migrated field*, P^m, obtained from a specific scalar component, P^0, of the EM field observed at the Earth's surface as being the field that satisfies the following conditions:

$$P^m(\vec{r},\tau)\,|_{z=0} = \begin{cases} P^0(r,T-\tau)_{z=0} & \text{for } 0 \le \tau \le T, \\ 0 & \text{for } \tau < 0,\ \tau > T \end{cases} \tag{3}$$

$$\Delta P^m(\vec{r},\tau) - \mu_0\sigma\frac{\partial P^m(\vec{r},\tau)}{\partial\tau} = 0 \text{ for } z > 0 \tag{4}$$

$$P^m(\vec{r},\tau) \to 0 \tag{5}$$

for $|\vec{r}| \to \infty$ $z>0$, where $\tau = T-t$ is a reverse time, T is an interval of EM signal recording.

Note that if we exchange reverse time, τ, for ordinary time, t, in eq. (4), we have an equation which is the adjoint to the diffusion equation:

$$\Delta P^m(\vec{r},t) + \mu_0\sigma\frac{\partial P^m(\vec{r},t)}{\partial t} = 0 \tag{6}$$

If the ordinary diffusion equation describes field propagation from the sources to receivers, then eq. (6) describes the inverse process of propagation from receivers to sources.

The problem of defining the migrated field reduces to the downward extrapolation of the field P^0 from the Earth's surface into the lower halfspace in the reverse time, τ. This procedure is called EM *field migration*.

It can be seen from these considerations, that the calculation of a migrated field is reduced to a boundary value problem described by eqs. (3) through (5). This boundary value problem can be solved, using Green's theorem and Green's function for the diffusion equation, G:

$$G(r',t' \mid r,t) = -\frac{(\mu_0\sigma)^{1/2}}{8\pi^{3/2}(t'-t)^{3/2}}e^{-\mu_0\sigma|r'-r|^2/4(t'-t)}H(t'-t) \tag{7}$$

Here $H(t'-t)$ is a Heaviside excitation function (step function):

$$H(t-t') = \begin{cases} 0; & t'-t < 0 \\ 1; & t'-t > 0 \end{cases}$$

Green's formula gives the following representation for the migrated field:

$$P^m(\vec{r}',T-r') = -2\int_{t'}^{T}\int\int_{-\infty}^{\infty} P^0(\vec{r},t)\frac{\partial\tilde{G}(\vec{r}',t' \mid \vec{r},\tau)}{\partial z}dxdydt \tag{8}$$

where $\tilde{G}$ is the adjoint to the Green's function G for the diffusion equation (Morse and Feshbach, 1953), (Zhdanov et al, 1988).

It is noteworthy that eq. (8) is the EM counterpart to the Rayleigh integral (Claerbout, 1985). Just as in the seismic application, eq. (8) defines in space and normal time a field propagating towards the surface of observation (that is, upgoing waves), as can be seen from the fact that eq. (8) contains the function G adjoint to the Green's function G of the diffusion equation. Hence, just as in the seismic case, a migration transformation of EM field yields the upgoing field.

Let us consider the special case of the 2D model of the EM field (for example the E polarised mode) and a profile observation. We assume that the axis X coincides with the profile, and axis Y is orthogonal to the profile of observations. In this case the expressions for the migration of the different components of the magnetic field, $H^0_{x,z}$ (x,0,t), observed along the profile X on the surface of the Earth, will have the form:

$$H^m_{x,z}(x',z',T-t') = \frac{\mu_0\sigma_n z'}{4\pi}\int_{t'}^{T}\int_X H^0_{x,z}(x,0,t)\frac{1}{(t-t')^2}\times \\ \times \exp\left\{-\frac{\mu_0\sigma_n}{4(t-t')}\left[(x'-x)^2+(z'-z)^2\right]\right\}dxdt \quad (9)$$

Note, that typical EM equipment uses receiver loops for measuring the components of magnetic field. Therefore, the actual data contains the records of EM induction in the loops which are proportional to the time derivatives of the magnetic field variations $\frac{\partial}{\partial t} H^0_{x,z}(x,0,t)$. Thus we have to modify (9):

$$\frac{\partial}{\partial t'}H^m_{x,z}(x',z',T-t') = \frac{\mu_0\sigma_n z'}{4\pi}\int_{t'}^{T}\int_X \frac{\partial}{\partial t}H^0_{x,z}(x,0,t)\frac{1}{(t-t')}\times \\ \times \exp\left\{-\frac{\mu_0\sigma_n}{4(t-t')}\left[(x'-x)^2+(z'-z)^2\right]\right\}dxdt \quad (10)$$

The last expression suggests the possibility in a 2D case of calculating the migrated electric field from the observed vertical component of the magnetic field.

From Maxwell's second equation for the migrated field we have:

$$\frac{\partial E^m_y}{\partial x} = -\mu_0\frac{\partial H^m_z}{\partial \tau}$$

and

$$E^m_y(\tilde{x},z',T-t') = \mu_0\int_{x_L}^{\tilde{x}}\frac{\partial}{\partial t'}H^m_z(x',z',T-t')dx' \quad (11)$$

where $(\tilde{x},z')$ is a current point of electrical field calculations, and x_L is a horizontal coordinate of the left end point on the profile.

Thus, from the observed vertical component of magnetic field we can calculate the migrated magnetic field at any level z, and then determine the migrated electric field E^m_y at the same level.

IMAGING OF GEOELECTRIC STRUCTURES BY TIME DOMAIN ELECTROMAGNETIC MIGRATION

For imaging the geoelectrical cross-section we can use the "EM radiating inhomogeneities" concept, analogous to the exploding-reflectors concept widely used in seismic migration. To illustrate this concept, we represent the observed EM field $\vec{E}$, $\vec{H}$ as being the sum of a primary field, $\vec{E}^p$, $\vec{H}^p$, *and a secondary field,* $\vec{E}^s$, $\vec{H}^s$:

$$\vec{E} = \vec{E}^p + \vec{E}^s, \quad \vec{H} = \vec{H}^p + \vec{H}^s \quad (12)$$

where the primary field is defined as being that field which is generated by a specific source in the Earth with the normal distribution of the electrical conductivity $\sigma_n(r)$ (e.g., in a homogeneous half-space) and the secondary field is due to the anomalous conductivity distribution. In another words we can treat the secondary field as the field generated by the extrinsic currents concentrated in inhomogeneous domains and layers.

It is noteworthy that a transfer in the integral formula (8) to the adjoint Green's function for the diffusion equation means that, as in the wave case, a field determined in the space by these integrals represents an assembly of EM ``waves" moving in the direction to the observation surface. However, in view of the specifics of the diffusion equation, this field does not feature such simple and effective geometrical properties as the Claerbout upgoing wave, ensuring a direct reconstruction of reflection boundaries by the location of fronts of a migration wave, at an instant t'=0. We will see nevertheless that the migrated EM field also can be used for the search for local inhomogeneities in a conducting medium, and for determination of geoelectrical boundaries.

To simplify our discussion we assume that the secondary field is generated by the pulse currents switching on at zero time. This field is propagating in different directions, and is observed on the surface of the Earth. The idea of EM migration consists of reverse downward extrapolation of the observed field in reverse time. Notice, that in the process of the reverse time extrapolation the time is decreasing. When the time reaches zero, the extrapolated field is at the source location. Thus, in the case of the secondary field this downward extrapolation in reverse time will result in focusing of the migrated field at zero time at it's source.

Note that in a real situation the behaviour of the sources of the secondary field is much more complicated than the pulse source. Also these sources "switch on" not at zero time, but after some delay related to the time of propagation of the primary field from the Earth's surface to the geoelectrical boundaries of inhomogeneties. For this reason we have two options: 1) to reconstruct the migration field in the lower halfspace not in zero time, but in the retarded times for different depth, or 2) to use for the downward extrapolation not the actual background conductivity, but instead some effective the *migration conductivity* σ_m proportional in the general case to the normal conductivity $\sigma_m=\gamma\sigma_n$, where γ is the so called *migration constant*. Detailed analysis of geoelectrical models shows that in the second case we can select the migration conductivity σ_m in such a way that the extreme point of the migration field in zero time coincides with the geoelectrical boundaries (see Appendix B).

It was shown in (Zhdanov and Booker, 1993) and (Zhdanov and Keller, 1994) that in the frequency domain secondary (upgoing) and primary (downgoing) fields everywhere inside the conducting layer are characterised by different amplitudes and phases. On the geoelectric boundaries their phases coincide (or shifted by π), while the amplitudes of the upgoing wave is proportional to the amplitude of the downgoing wave and the proportionality factor is equal to the reflectivity coefficient β. When passing into the time domain the above regularities manifest themselves in the fact that the shapes of a time pulse of upgoing and downgoing waves everywhere inside the conducting layer differ and are coincident (simply mutually proportional to the coefficient β) only at the geoelectric boundary (see Appendix A).

We can introduce a time domain apparent reflectivity function, $\beta_{ta}(\vec{r},t)$, defined as the ratio of secondary $E^s_y(\vec{r},t)$ and primary $E^p_y(\vec{r},t)$ fields, as follows:

$$\beta_{ta}(\vec{r},t) = E_y^s(\vec{r},t)/E_y^p(\vec{r},t) \tag{13}$$

The determination of this function, obviously, relies upon the procedure used for downward extrapolation of the upgoing and downgoing fields in the lower half space. However, it can be generalised to the results of time domain EM migration.

In Appendix A we show that the migration apparent reflectivity function at zero time $\beta_a^{\mu}(\vec{r})$ can be determined also from the values of the migrated secondary field, calculated in zero time and normalised by some function $D(\vec{r})$:

$$\beta_a^m(\vec{r}) = E_y^{ms}(\vec{r},0)/D(\vec{r}) \tag{14}$$

where $D(\vec{r})$ is the convolution of the migrated primary field at the same depth and the analytical function $\varphi(z,t)$

$$D(\vec{r}) = D(x,z) = \int_0^{+\infty} H_z^{mp}(x,z,t)\varphi(z,t)\,dt \tag{15}$$

where

$$\varphi(z,t) = a\frac{z}{\tau^3}\exp\left[-2\pi^2\left(\frac{z}{\tau}\right)^2\right] \tag{16}$$

In the last equation:

$$a = \frac{2^{7/2}\pi^{5/2}}{\mu\sigma_n};\ \tau = 2\pi\sqrt{2t/\mu\sigma_n} \tag{17}$$

The function β_a^m is equal to the actual reflectivity coefficient β exactly at the position of the boundary:

$$\beta_a^m(\vec{r}) = \beta \tag{18}$$

This result is based on the fact that the migrated secondary (upgoing) field has local extreme point exactly at the location of geoelectric boundaries. This extreme point is proportional to the reflectivity of the boundary and to the magnitude of the downgoing (primary) field at the same point.

The reflectivity coefficient is connected with the conductivity contrast $\Delta\sigma$ at the geoelectrical boundary by a simple formula (see eq. (19) of the Appendix A):

$$D(\vec{r}) = D(x,z) = \int_0^{+\infty} H_z^{mp}(x,z,t)\varphi(z,t)\,dt$$

From this we can determine the resistivity $\rho=1/(\sigma_n+\Delta\sigma)$ below the geoelectrical boundary (within the anomalous domain or layer):

$$\rho = \left[\frac{1+\beta}{1-\beta}\right]^2 \rho_n \tag{19}$$

where ρ_n is the background (normal) resistivity. The last expression gives the exact value of the resistivity of the second layer in the framework of the 2-layered model with the slow horizontal variation of conductivity (see Appendix A). However, following the traditional approach to electrical sounding , we can use this expression for an arbitrary model. In this case we will call the corresponding value of the resistivity, computed by eq. (19), *the migration apparent resistivity.*

So, the migration apparent resistivity ρ_m can be calculated using the formula:

$$\rho_m(\vec{r}) = \left\{\frac{[1+\beta_a^m(\vec{r})]}{[1-\beta_a^m(\vec{r})]}\right\}^2 \rho_n(\vec{r}) \tag{20}$$

We emphasise that the migration apparent resistivity ρ_m is a function of depth. Thus we obtain the depth geoelectrical cross section.

Note, that the migrated secondary field in the expression (14) is calculated at zero time, that corresponds to secondary field propagation in the vicinity of the source location. We can compare this situation with the time domain sounding, when the depth of the field penetration inside the Earth is proportional to the square root of the time after the current pulse in the transmitter: for early times the field is concentrated in near surface layers, for later times the field penetrates deeper in the Earth. In the case of the migrated field at early times this field is in the vicinity of its sources - geoelectrical boundaries. At later times this field propagates upward to the Earth's surface. Thus at early time the migrated field behaviour is determined only by the properties of the medium near the boundary between two layers. Therefore we can successfully use eq. (19) for determining the conductivity contrast between these layers.

In the case of multilayered cross sections we can start from the first layer and determine the resistivity of the second layer, then find the conductivity contrast between second and third layer and determine the resistivity of the third layer, etc. This layer by layer process opens the way for direct imaging of the complex geoelectrical structures. In a model with a complex multilayered structure we can take as ρ_n the apparent resistivity of the Earth $\rho_a(t)$ obtained by the corresponding formulae of the theory of EM soundings and averaged along the profile of observations. The time t of the apparent resistivity calculation can be connected with the depth of downward extrapolation d by the following approximate expression for the skin-depth (Zhdanov and Keller, 1994):

$$d \approx \sqrt{2t\rho_a(t)/\mu_0} \tag{21}$$

In the framework of this approach an inhomogeneous profile of the Earth's resistivity is substituted by some homogeneous model which is used as background (normal) resistivity for the migration (for each depth d – by its own). We call this normal resistivity profile the model of the mean resistivity.

This approach is similar to one used in seismic prospecting when the real velocity distribution is substituted by the model of the mean velocity (Claerbout, 1985). Also, as in seismic

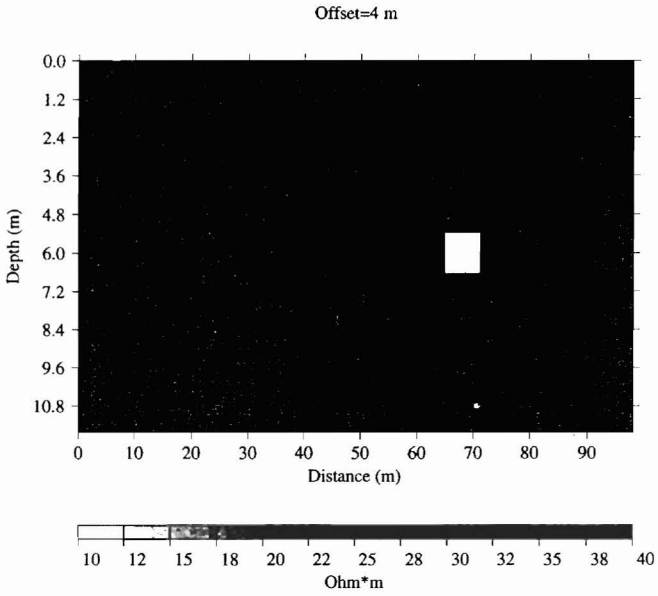

Fig. 1. Geoelectrical cross section of the test model, containing a highly conducting inclusion (on the right) and a poorly conducting inclusion (on the left). The EM field in the model was generated by an infinitely long cable. The observed field was dH_z/dt.The theoretical survey was conducted in the transmitter offset mode with the transmitter - receiver separation (offset) equal to 4m.

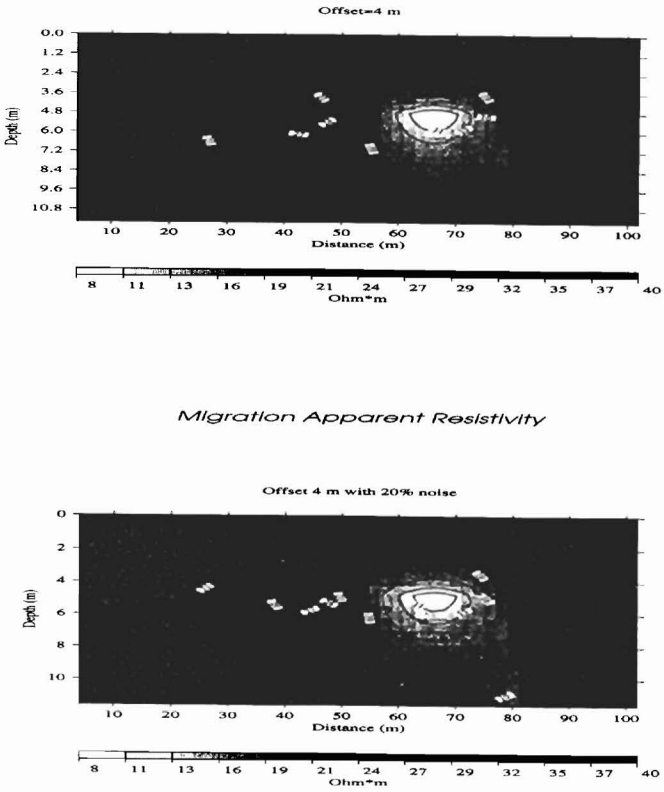

Fig. 2. The migration apparent resistivity cross section in time domain, computed from the migration electric field for the model in Figure 1 (top panel). The same results for data with 20% white noise added to the secondary field dH_z/dt (bottom panel).

prospecting we can use the recursive algorithms of migration which are based on successive downward extrapolation from level to level with different background resistivity.

NUMERICAL MODELING

The resistivity imaging technique has been tested on the results of numerical modeling with the use of a 2D finite-difference time domain code (Oristaglio and Hohmann, 1984). Figure 1 shows the geoelectrical cross section of the model, containing a highly conducting inclusion (on the right) and a poorly conducting inclusion (on the left). The EM field in the model was generated by an infinitely long cable. The observed field was dH_z/dt. The theoretical survey was conducted in the transmitter offset mode with the transmitter - receiver separation (offset) equal to 4 m. The results of TDEM migration of the secondary field dH_z/dt were than recalculated in the migration electric field. This field has been used to compute the migration apparent resistivity in the time domain (Figure 2, top panel).

To examine the effect of noise, we have added 20\% white noise to the secondary field dH_z/dt computed on the Earth's surface. The results of the migration of this noisy data illustrate the stability of the migration. Migration apparent resistivity, calculated from the noisy data (Figure 2, bottom panel), is very close to the resistivity image presented on the Figure 2, top panel.

CASE HISTORY: INTERPRETATION OF RWMC TDEM DATA

This method has been applied for waste site characterisation, using TDEM data. The main task was the interpretation of the time domain electromagnetic (TDEM) data set acquired at the Cold Test Pit site within the Radioactive Waste Management Complex (RWMC) at the Idaho National Engineering Laboratory (INEL) (Mac Lean, 1993). The Cold Test Pit was specially designed to test the different geophysical methods. So, we knew a priori the internal structure of the pit and could check the results of migration. A schematic plan of the Pit is presented at the Figure 3. We have processed by TDEMM Method data obtained as a result of high density TDEM profiling survey using a Geonics EM47 instrument along a set of profiles, crossing INEL RWMC Cold Test Pit from the West to the East. The survey was conducted in the transmitter offset or slingram mode as described in (Mac Lean, 1993). The transmitter - receiver separation (distance between the center of the transmitter loop and receiver loop) was equal to 12.5 m. The geoelectrical structure of the pit is three dimensional, making it impossible to use the conventional methods to interpret these data.

We have processed 13 profiles, numbered from the North to the South (see Figure 3): 15N, 0S, 5S, 10S, 15S, 20S, 25S, 30S, 35S, 40S, 45S, 50S, 60S. We have used as an effective

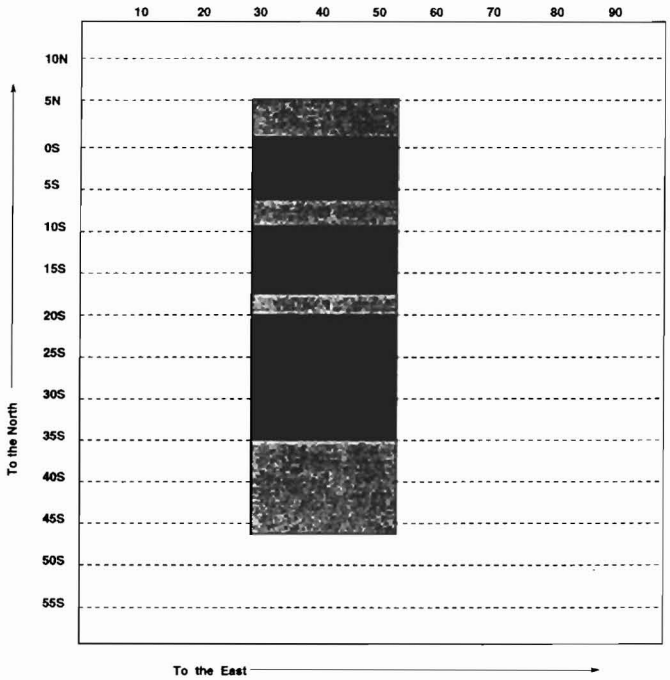

Fig. 3. The schematic plan of the RWMC Cold Test Pit. 1 - nonconductive zones (Earth berm); 2 - conductive zones (random dump drums and boxes); 3 - conductive zone (stacked drums, contains 700 drums).

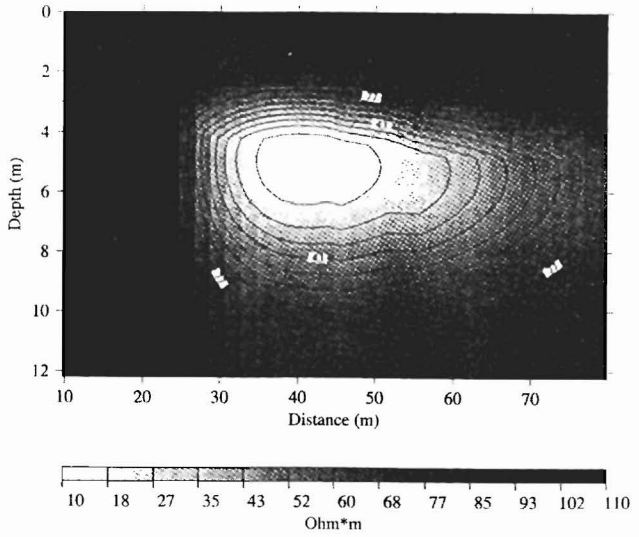

Fig.4. Time domain migration resistivity cross sections interpolated in the horizontal planes to produce horizontal maps of the resistivity distribution at depth 3 m (top panel) and 5 m (bottom panel). Solid line on these maps shows the known boundary of the RWMC Cold Test Pit.

background resistivity ρ_n=100 *Ohm* · m. As a result of processing of TDEM data using the migration method we have obtained a set of vertical cross sections of the Cold Test Pit. The typical cross section of the migration apparent resistivity along the profile 35S is presented on the Figure 4. These data have been interpolated in horizontal planes to plot the horizontal variations of the resistivity at different depths, specifically, 2, 3, 4, 5, 6, 7, 8 and 9 m. We present here, as an example, the resistivity maps at depths 3 and 5 m. (Figure 5). The solid lines on these maps show the known boundary of the pit. Consider, for example, the migration resistivity map at a depth 5 m (Figure 5, bottom panel). We observe on this map several conductivity anomalies that correlate very well with the pit sections filled with the drums and boxes full of waste. Note, that elongation of the anomalous conductive zone in the northern section of the pit outside the formal boundary of the pit can be explained by the interpolation effects between profiles 15N and 0S. In fact, there is no profile between profiles 15N and 0S. So, conductive structure from profile 0S could be formally extrapolated outside the pit by the interpolation code. However, comparing the maps on Figure 5 with known Pit scheme (Figure 3) we can see that in general the internal structure of the pit is reflected reasonably well on these maps.

We have also constructed 3D resistivity image on the basis of resistivity maps at depth 2, 4, 6, and 8 m (Figure 6). One can see on these maps that conductive structures appear at depth bellow 2 m and disappear at depth about 8 m. The maximum of the conductive structures on the resistivity images lies at depth about 5 m. This picture provides a reasonable volume image of the pit that corresponds well to the known internal structure of the pit (Mac Lean, 1993). Thus the results of the time domain EM migration and resistivity imaging demonstrate that this method can be used to determine the structure of anomalous resistivity distribution in INEL RWMC Cold Test Pit.

CONCLUSION

TDEM migration and resistivity imaging made it possible to interpret TDEM sounding data in the areas with horizontally inhomogeneous geological structures. This problem cannot be solved using conventional 1D inversion techniques.

TDEMM is a tool to locate anomalous geoelectric zones and determine the resistivities. The resistivity images can be obtained only on the basis of the vertical component of magnetic field H_z observations in the transmitter offset or slingram mode.

The TDEMM is a stable and fast method of geoelectrical imaging. It doesn't require costly forward modeling as do conventional inversion techniques. However, the main limitations of migration are due to the necessity for spatially dense measurements of EM responses along the profile or over surface of the Earth.

ACKNOWLEDGMENTS

We thank the Consortium on Electromagnetic Modeling and Inversion at the Department of Geology and Geophysics, University of Utah, for providing support for this work. We also wish to thank Dr. H. D. Mac Lean for providing the TDEM data and the fruitful discussions regarding results of migration and resistivity imaging.

REFERENCES

Barnett, C.T., 1984, Simple inversion of time-domain electromagnetic data: Geophysics, **49**, 925-933.

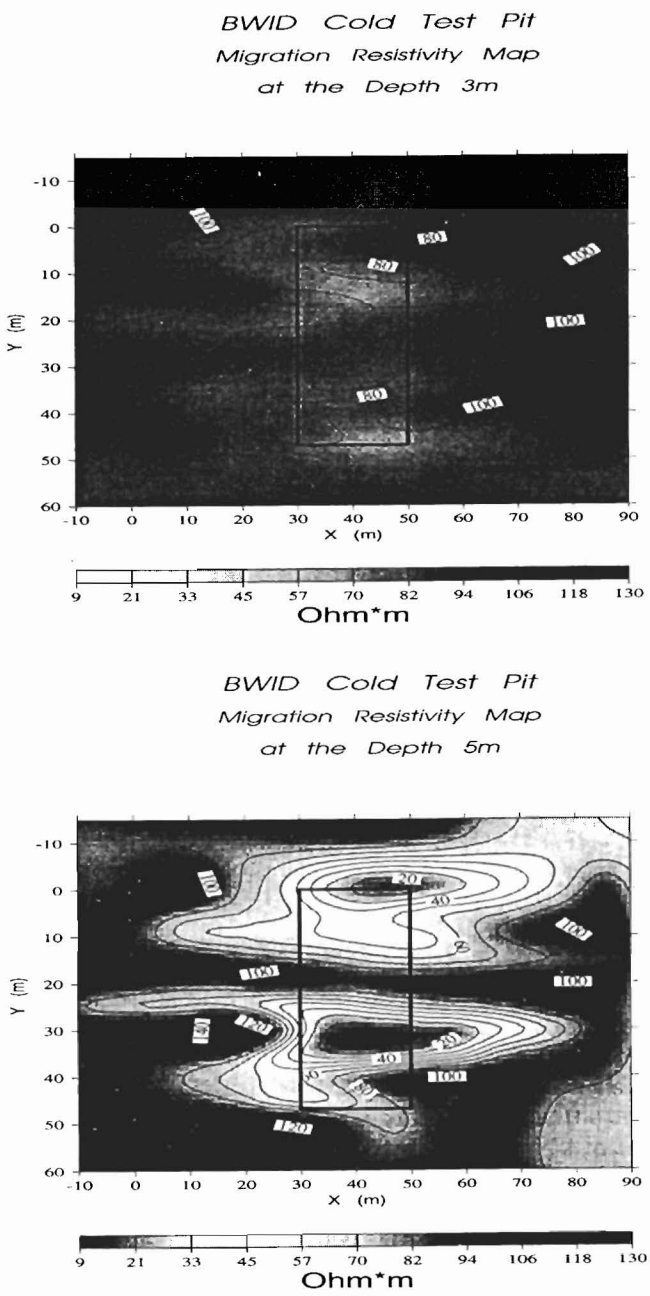

Fig. 5. Vertical cross section of the migration apparent resistivity along the profile 35S.

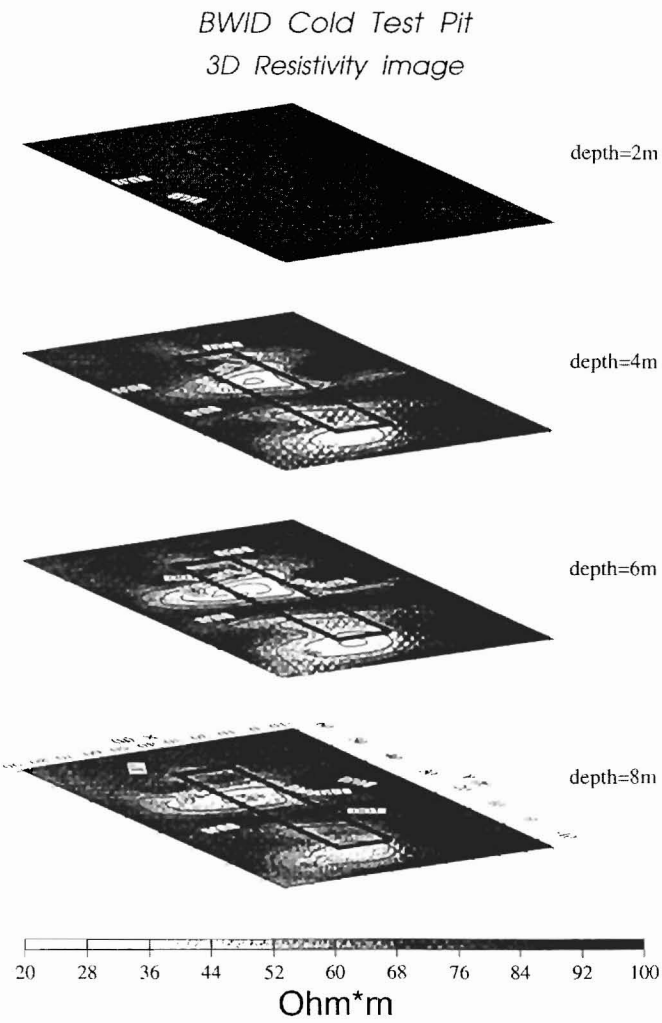

Fig. 6. 3D resistivity images of the RWMC Cold Test Pit, constructed on the basis of resistivity maps at depth 2, 4, 6, and 8 m.

Claerbout, J.F., 1985, Imaging the Earth Interior. Blackwell Sci. publ., Oxford, 399p.

Eaton, P.A. and Hohmann, G.W., 1989, A rapid inversion technique for transient electromagnetic soundings: PEPI, **53**, 384-404.

Macnae, J., and Lamontagne, Y., 1987, Imaging quasi-layered conductive structures by simple processing of transient electromagnetic data. Geophysics, **52**, 545-554.

Mac Lean H.D. 1993, Time domain electromagnetic survey of three waste burial pits at INEL Radioactive Waste Management Complex, TTP AL 911201-G2, Chem-Nuclear Geotech, Inc.

Morse, P.M., and Feshbach, U., 1953, Methods of Theoretical Physics: McGrawHill Book Co., New York, 1978 p.

Nabighian, M.N., 1979, Quasi-static transient response of a conducting half-space - an approximate representation. Geophysics, **44**, 1700-1705.

Oristaglio, M., and Hohmann, G., 1984, Diffusion of electromagnetic fields into a two-dimensional Earth: A finite-difference approach: Geophysics, **49**, 870-894

Zhdanov, M.S., 1988, Integral transforms in geophysics, Springer, Berlin, 367 p.

Zhdanov, M.S., Matusevich, V.U., and Frenkel, M.A., 1988, Seismic and Electromagnetic Migration (in Russian): Nauka, Moscow, 374 p.

Zhdanov, M.S., and Booker, J.R., 1993, Underground Imaging by Electromagnetic Migration, 63 SEG Annual meeting, Expanded abstracts, p. 355-357

Zhdanov, M.S., and Keller, G.V., 1994, The Geoelectrical Methods in Geophysical Exploration. Elsevier, Amsterdam, 873 p.

Zhdanov, M.S., Traynin, P. and Booker, J.R., 1994, Underground Imaging by Frequency Domain Electromagnetic Migration (submitted to Geophysics).

APPENDIX A: MIGRATION APPARENT RESISTIVITY

Consider a 2D model of the EM field (E-polarisation). It is important to notice that in the model with slow horizontal variation of the conductivity and of the field, we can represent the different components of the EM field in the frequency domain approximately by the following formulae (Zhdanov et al, 1994)

$$H_{x,z}(x,z,\omega) = Q^p_{x,z}(x,z,\omega)e^{ik_n z} + Q^s_{x,z}(x,z,\omega)e^{-ik_n z}$$

$$E_y(x,z,\omega) = Q^p_y(x,z,\omega)e^{ik_n z} + Q^s_y(x,z,\omega)e^{-ik_n z} \qquad (22)$$

where $Q^{p,s}_{x,y,z}$ are the coefficients relatively slow depending on the depth, $H_{x,z}(x,z,\omega) = Q^p_{x,z}(x,z,\omega)e^{ik}$ is a wave number and $\sigma_n(x,z)$ is a background conductivity.

Here the terms associated with the downgoing exponential function correspond to the primary field and the terms associated with the upgoing exponential function correspond to the secondary field:

$$H^p_{x,z}(x,z,\omega) = Q^p_{x,z}(x,z,\omega)e^{ik_n z},\quad H^s_{x,z}(x,z,\omega) = Q^s_{x,z}(x,z,\omega)e^{-ik_n z} \tag{23}$$

$$E^p_y(x,z,\omega) = Q^p_y(x,z,\omega)e^{ik_n z},\quad E^s_y(x,z,\omega) = Q^s_y(x,z,\omega)e^{-ik_n z}$$

Let us consider, for the sake of simplicity, the two-layered model with the slow variation of conductivity $\sigma_n(x,z)$ and $\sigma_{n+1}(x,z)$ within each layer and sharp conductivity contrast on the quasi horizontal boundary S between two layers.

We will analyse the behaviour of the horizontal component of the electric field at the quasi-horizontal boundary $\{S : (x,d(x))\}$ between two layers. In the 1st layer we have:

$$E_y(x,d,\omega) = Q^p_y(x,d,\omega)e^{ik_n d} + Q^s_y(x,d,\omega)e^{-ik_n d} \tag{24}$$

$$E'_y(x,d,\omega) = ik_n Q^p_y(x,d,\omega)e^{ik_n d} - ik_n Q^s_y(x,d,\omega)e^{-ik_n d}$$

while in the second layer:

$$E_y(x,d,\omega) = Q_y(x,d,\omega)e^{ik_{n+1}d} \tag{25}$$
$$E'_y(x,d,\omega) = ik_{n+1}Q_z(x,d,\omega)e^{ik_{n+1}d}$$

where "prime" means the vertical derivative of the electric field.

On the boundary S in the case of E-polarization both components E_y and E'_y are continuous. Therefore, the corresponding right-hand sides of (24) and (25) are equal. Solving this system of equation, we find:

$$\frac{Q^s_y}{Q^p_y} = \beta(x,d)\,e^{2ik_n d} \tag{26}$$

where

$$\beta(x,d) = \frac{\sqrt{\sigma_n(x,d)} - \sqrt{\sigma_{n+1}(x,d)}}{\sqrt{\sigma_n(x,d)} + \sqrt{\sigma_{n+1}(x,d)}} \tag{27}$$

is the so-called *reflectivity coefficient*. Let us calculate the frequency domain apparent reflectivity function as the ratio of the secondary and primary fields:

$$\beta_a(x,z,\omega) = \frac{E^s_y(x,z,\omega)}{E^p_y(x,z,\omega)} = \frac{Q^s_y(x,z,\omega)}{Q^p_y(x,z,\omega)}e^{-2ik_n z} \tag{28}$$

According to (26) at the boundary:

$$\beta_a(x,d,\omega) = \beta(x,d) \tag{29}$$

So, at the geoelectrical boundary apparent reflectivity function is equal exactly to the true reflectivity coefficient!

Now let us find the way to calculate the apparent reflectivity function from the migrated fields. According to the definition (Zhdanov et al. 1994), the migrated secondary and primary fields (E^{ms}_y and E^{mp}_y) can be expressed approximately as :

$$E^{ms}_y(x,z,\omega) = Q^s_y(x,z,\omega)e^{-k_m z},\ E^{mp}_y(x,z,\omega) = Q^p_y(x,z,\omega)e^{-k_m z} \tag{30}$$

where $k_m(x,z,\omega) = \sqrt{i\omega\mu_0\sigma_m(x,z)}$ is a migration wave number.

According to eq. (28), (29) and (30) the fields E^{ms}_y and E^{mp}_y are proportional at the boundary S:

$$E^{ms}_y(x,d,\omega) = \beta(x,d)\,E^{mp}_y(x,d,\omega)e^{2ik_n d} \tag{31}$$

Equation (31) can be used for calculation of the time domain migration apparent reflectivity function $\beta^m_{ta}(x,z,t)$ at zero time:

$$\beta^m_a(x,z) = \beta^m_{ta}(x,z,t=0) = \frac{E^{ms}_y(x,z,t=0)}{D(x,z)} \tag{32}$$

Here $\beta^m_{ta}(x,z,t)$ is obtained from the ratio $\frac{E^{ms}_y(x,z,\omega)}{E^{mp}_y(x,z,\omega)}$ by inverse Fourier transform from frequency domain to time domain, and $D(x,z)$ and $\varphi(z,t)$ are determined by equations (15) and (16).

The function $\beta^m_a(x,z)$ is equal to the actual reflectivity coefficient β exactly at the position of the boundary:

$$\beta^m_a(x,d) = \beta(x,d) \tag{33}$$

APPENDIX B: EXTREME POINT PROPERTIES OF THE MIGRATION FIELD.

Next simplification of the model is based on the assumption that the coefficient $Q^p_y(x,z,\omega)$ in the equation (23) doesn't depend on ω and very slowly changes with z:

$$Q^p_y(x,z,\omega) \approx Q_0(x) \tag{34}$$

These conditions for example take place in the case of constant conductivity of the first layer and if the primary field can be approximated by the plane wave with a δ-pulse waveform on the surface of the Earth. Under these conditions we can write approximately:

$$E^p_y(x,z,\omega) = Q_0(x)\,e^{ik_n z} \tag{35}$$

Therefore from (26) and (23) we have:

$$E_y^p(x,z,\omega) = Q_0(x)\, e^{ik_n z} \tag{36}$$

According to definition the migrated secondary field in frequency domain is equal to

$$E_y^{ms}(x,z,\omega) = Q_0(x)\,\beta(x,d)\, e^{2ik_n d} e^{-k_m z} \tag{37}$$

If we apply the inverse Fourier transform from frequency domain to time domain, we find the migrated secondary field in time domain:

$$E_y^{ms}(x,z,t) = \frac{1}{2\pi} Q_0(x)\,\beta(x,d) \int_{-\infty}^{+\infty} e^{2ik_n d} e^{-k_m z} e^{-i\omega t} d\omega \tag{38}$$

The last integral can be reduced to the tabulated one, if t=0. Omitting long calculations, we write:

$$E_y^{ms}(x,z,t=0) = -\frac{8Q_0(x)\,\beta(x,d)\, d\gamma^{1/2} z}{\pi\mu\sigma_1 \left(4d^2 + \gamma z^2\right)^2} \tag{39}$$

where $\gamma = \sigma_m/\sigma_n$ is the migration constant.

Let us find now the depth of the extreme point of the migration field:

$$\frac{\partial}{\partial z} E_y^{ms}(x,z,t=0) = -\frac{8Q_0(x)\,\beta_{12}(x,d)\, d\gamma^{1/2} z}{\pi\mu\sigma_1 \left(4d^2 + \gamma z^2\right)^3} \left(4d^2 - 3\gamma z^2\right) \tag{40}$$

One can see that the vertical derivative of the migrated field is equal to zero exactly at the depth of the boundary z = d, if migration constant γ = 4/3. The value of the migration field in the extreme point is equal to:

$$E_y^{ms}(x,d,t=0) = -\frac{\sqrt{3}Q_0(x)\beta(x,d)}{4\pi\mu\sigma_m d^2} \tag{41}$$

From the last formula we can find $\beta(x,d)$:

$$\beta(x,d) = -\frac{4\pi\mu\sigma_m d^2}{\sqrt{3}Q_0(x)} E_y^{ms}(x,d,t=0) \tag{42}$$

and calculate the resistivity of the second layer:

$$\rho_{n+1}(x) = \left[\frac{1+\beta(x,d)}{1-\beta(x,d)}\right]^2 \rho_n \tag{43}$$

Expression (43) gives the exact solution for the problem of the determination of $\rho_{n+1}(x)$ only for this simple model under consideration. However, following traditional approach to EM sounding, we can introduce migration apparent resistivity, which is determined by the same formula:

$$\rho_m(x,z) = \left[\frac{1+\beta_a^m(x,z)}{1-\beta_a^m(x,z)}\right]^2 \rho_n \tag{44}$$

In the last expression $\beta_a^m(x,z)$ is given by eq. (32).

Note in the conclusion that expression (42) can be obtained directly from equations (32) and (15).